Self-Assembled Microstructures of Confined Rod−Coil Diblock Copolymers by Self-Consistent Field Theory

Guang Yang,[‡,†] Ping Tang,*[‡,†] Yuliang Yang,[‡,†] and Qiang Wang[‡,§]

Key Laboratory of Molecular Engineering of Polymers of Ministry of Education and Department of Macromolecular Science, Fudan University, Shanghai 200433, China, and Department of Chemical and Biological Engineering, Colorado State University, Fort Collins, Colorado 80523-1370, United States

Received: August 23, 2010; Revised Manuscript Received: October 8, 2010

We employ the self-consistent field theory (SCFT) incorporating Maier−Saupe orientational interactions between rods to investigate the self-assembly of rod−coil diblock copolymers (RC DBC) in bulk and especially confined into two flat surfaces in 2D space. A unit vector defined on a spherical surface for describing the orientation of rigid blocks in 3D Euclidean space is discretized with an icosahedron triangular mesh to numerically integrate over rod orientation, which is confirmed to have numerical accuracy and stability higher than that of the normal Gaussian quadrature. For the hockey puck-shaped phases in bulk, geometrical confinement, i.e., the film thickness, plays an important role in the self-assembled structures' transitions for the neutral walls. However, for the lamellar phase (monolayer smectic-C) in bulk, the perpendicular lamellae are always stable, less dependent on the film thicknesses because they can relax to the bulk spacing with less-paid coil-stretching in thin films. In particular, a very thin rod layer near the surfaces is formed even in a very thin film. When the walls prefer rods, parallel lamellae are obtained, strongly dependent on the competition between the degree of the surface fields and film geometrical confinement, and the effect of surface field on lamellar structure as a function of film thickness is investigated. Our simulation results provide a guide to understanding the self-assembly of the rod−coil films with desirable application prospects in the fabrication of organic light emitting devices.

Introduction

Rod−coil diblock copolymers (RC DBC) can self-assemble into various nanostructures with rod and coil segments forming acceptor and donor domains, respectively,[1,2] providing an efficient and economic way to fabricate polymeric organic optoelectronics compared with conventional devices.[3] To obtain high values of photocurrent, recent studies in experiments[4] and theory[5] revealed that the length scale of the microdomains formed by the rod−coil block copolymers, the self-assembled morphologies and the arrangement of the rod orientation between two electrodes have great influences on the efficiencies and brightness of the exciton splitting and electron transport. Many applications of rod−coil block copolymers, such as organic photovoltaics, require both creation of nanoscale structure and detailed pattern formation in thin films.[6,7] Although it is clear that the spatial confinement and the interactions between the block species and confining surfaces can be used to control the self-assembled morphologies and induce long-range ordering of the microdomains for coil−coil block copolymers,[8−12] the equilibrium structures of rod−coil block copolymers self-assembled in thin films are difficult to obtain in experiments because aggregate structures form in solution and the morphologies are kinetically trapped in the film during deposition.[7] Furthermore, the flat surfaces and the different surface selectivity to the two blocks play an important role in the orientation of the rods near the surfaces and the morphologies of the films.[7,13] Therefore, theory and computer simulation can help us understand the equilibrium morphologies of RC DBC confined in thin films.

For block copolymers in the intermediate segregation region, self-consistent field theory (SCFT) has proved to be one of the most successful theoretical methods for investigating equilibrium phases of block copolymers in bulk[14,15] and under confinement.[9,12] At present, SCFT has played a major role in characterizing the phase behavior of Gaussian chain systems, whereas the application of numerical SCFT studies on the self-assembly of RC DBC is quite limited. Muller and Schick[16] studied the phase behavior of RC DBC by applying a partial numerical evaluation of the single chain partition function in the weak segregation limit and a brushlike approximation in the strong segregation limit and found that the phases with the coils on the convex side of the rod−coil interface are the only stable morphologies. Matsen and Barrett[17] performed the SCFT calculations of RC DBC, in which the coil blocks are treated as continuous Gaussian chains and the rod blocks as rigid rods using the Semenov−Vasilenko[18] model. The wormlike chain model[19,20] has been commonly used to describe the chain rigidity, which requires an additional quantity, namely a unit vector defined on a spherical surface, for describing the orientation of rod segments. This chain model renders 6D space chain propagator $q(\mathbf{r},\mathbf{u},s)$ composed of a 3D position space, 2D orientation space, and chain contour s, which is quite difficult to solve numerically. At present, the studies on the self-assembled RC DBC modeled by wormlike chain are almost limited in 1D position space. Netz and Schick[21] studied symmetric block copolymers modeled by continuous wormlike chain model with dipolar and quadrupolar interactions. Shah and Ganesan[22] studied the chain bridging in lamellae of symmetric tri- and pentablock copolymers consisting

* Corresponding author. E-mail: pingtang@fudan.edu.cn.
† Department of Macromolecular Science, Fudan University.
‡ Key Laboratory of Molecular Engineering of Polymers of Ministry of Education, Fudan University.
§ Colorado State University.

10.1021/jp107997b
Published on Web 11/03/2010

of rod and coil blocks modeled by a continuous wormlike chain and continuous Gaussian chain, respectively with Maier−Saupe type for describing rod orientational interaction. So far, only two 2D SCFT studies for self-assembled rod−coil block copolymers have been reported: Hamm[23] et al. performed dynamic mean-field method for RC DBC modeled by discrete wormlike chain and found the hockey puck micelles, smectic-C and smectic-A phases with increasing volume fraction of the rod block. Using a more tractable model of continuous rigid rod for the rod blocks and continuous Gaussian chain for the coil blocks, Pryamitsyn and Ganesan[24] performed 2D SCFT calculations of RC DBC with incompressibility constraint, and found nematic, smectic-A, smectic-C, arrowheads, puck-shaped phase, broken lamella, and bilayer phases.

However, only a few theoretical studies[25−27] have investigated the self-assembled morphologies of RC DBC under confinement, most of which were restricted to analytical solutions with some assumptions. Pereira and Williams[25] reported that smectic rod−coil melts confined between two flat surfaces are much more constrained than the analogous coil−coil system, and the perpendicular lamellae are observed in relatively thick films for certain values of rod−coil interfacial tensions. Cheng and Cao[26] used density functional theory (DFT) to prove that the smectic-A to smectic-C translation is driven by the copolymer bulk concentration. The slit width and molecular flexibility also influence the self-assembled structures in film. Nowak and Vilgis[27] carried out an extended scaling method to characterize the aggregates of RC DBC adsorbed at a surface, indicating that the aggregate of rods is parallel to the surface allowing for the chain to gain entropy. Quite recently, the photovoltaic properties of rod−coil block copolymers was reported by Shah and Ganesan,[5] on the basis of their previous SCFT framework.[24] In addition to the theoretical studies, conformational changes of the semiflexible polymers induced by surfaces have been performed by DFT simulation,[28] Monto Carlo simulation,[29,30] and Langevin simulations.[31] These studies indicate the different behavior of semiflexible polymers near surfaces from that of flexible polymers.

In this article, we employ the same theoretical model as that of Pryamitsyn and Ganesan:[24] a copolymer chain model where the coil blocks are treated as continuous Gaussian chains and the rod blocks as continuous rigid rods, and a pseudospectral SCFT based on the two-order parameter approach proposed by Holyst and Schick[32] with the isotropic Flory−Huggins interaction between rod and coil blocks and anisotropic Maier−Saupe orientational interactions between rod components. Differently from ref 24, however, we discretize the orientation of a rod block **u** defined on a unit sphere with an icosahedron triangular mesh, which has been confirmed to have high numerical stability in our previous work to study the phase separation of diblock copolymers on spherical surfaces[33] and the self-assembly of semiflexible diblock copolymers with SCFT.[34] Our icosahedron triangular mesh discretization describes the rod orientations in 3D space more accurately than the coarser discretization of rod orientation with Gaussian quadrature for angular integrals used by Pryamitsyn and Ganesan.[24] We further study the self-assembly of RC DBC confined between two identical and flat surfaces, where the volume fraction of the coil block is fixed as $f = 0.4$ and $f = 0.6$; the confinement effect on the phase behavior of the rod−coil system is systematically investigated as a function of the orientation interaction between rod blocks, the Flory−Huggins interaction between the rod and coil segments, the size asymmetry of the rod and coil segments, and the surface preference.

Theoretical Formalism

In this section, we briefly describe the SCFT theoretical framework for predicting the equilibrium structures of rod−coil diblock copolymers confined between two horizontal symmetrical hard surfaces. The derivation in detail is similar to the SCFT for RC DBC in bulk described by Pryamitsyn and Ganesan.[24] Considering that incompressible rod−coil diblock copolymer melts consist of n identical copolymer chains in volume V. Each coil block has N_C segments with their statistical segment length a, and each rod block has N_R segments with the length of each rod segment $b = l_R/N_R$, where l_R is the length of each rod block. For simplicity, the rod and coil segments are assumed as the same bulk number density $\rho_0 = nN/V$, where $N \equiv N_C + N_R$ denotes the copolymer chain length in each copolymer chain. Therefore, the volume fraction of the coil block is $f = N_C/N$ and $1 - f$ for the rod block. In the SCFT, the copolymer is parametrized with a continuous path variable s (in units of N), which increases from $s = 0$ at the beginning of the A block to $s = f$ at the junction of the two blocks and to $s = 1$ at the end of the B block. The conformation of the flexible A block is described by the continuous Gaussian chain model, and the orientation of the rigid B block in the kth chain is described by a unit vector $\mathbf{u}_k$ (pointing from $s = f$ to $s = 1$). The fundamental quantity to be calculated in mean field studies is the polymer segment probability distribution function, $q(\mathbf{r},s)$, representing the probability for a partial chain of length $s \le f$ starting from the coil-end (where $s = 0$) anywhere in the system and end at position $\mathbf{r}$. It satisfies a modified diffusion equation according to a flexible Gaussian chain model:[35]

$$\frac{\partial q(\mathbf{r},s)}{\partial s} = \nabla^2 q(\mathbf{r},s) - \omega_C(\mathbf{r})\, q(\mathbf{r},s) \qquad 0 < s \le f \tag{1}$$

where the length of the system is scaled by $R_g \equiv a(N/6)^{1/2}$. $\omega_C(\mathbf{r})$ is the potential field conjugate to the volume fraction of the coil block. The initial condition is $q(\mathbf{r},0) = 1$. Similarly, the other segment probability distribution function $q^*(\mathbf{r},s)$ corresponds to the probability for a partial copolymer chain of length s that starts from the joint end of two blocks (where $s = f$) and end at position $\mathbf{r}$, irrespective of the orientation of the rod block. It satisfies the modified diffusion equation:

$$\frac{\partial q^*(\mathbf{r},s)}{\partial s} = -\nabla^2 q^*(\mathbf{r},s) + \omega_C(\mathbf{r})\, q^*(\mathbf{r},s) \qquad 0 < s \le f \tag{2}$$

The initial condition is

$$q^*(\mathbf{r},s=f) = \frac{\int d\mathbf{u} \exp[-\int_0^{1-f} ds\, \Gamma(\mathbf{r} + \beta s\mathbf{u},\mathbf{u})]}{\int d\mathbf{u}} \tag{3}$$

where $\beta = Nb/(a^2N/6)^{1/2} = 6^{1/2}\nu^{-1}$ ($\nu = aN^{1/2}/bN$) denotes the size asymmetry ratio. $\Gamma(\mathbf{r},\mathbf{u})$ is given

$$\Gamma(\mathbf{r},\mathbf{u}) \equiv \omega_R(\mathbf{r}) - \mathbf{M}(\mathbf{r}):\left(\mathbf{uu} - \frac{\mathbf{I}}{3}\right) \tag{4}$$

where $\omega_R(\mathbf{r})$ is the potential field conjugate to the volume fraction of rods. $\mathbf{I}$ is a 3×3 identity matrix. $\mathbf{M}(\mathbf{r})$ is the conjugate tensorial orientation field.

We follow the "masking" technique proposed by Fredrickson et al.[36] and adopted later in our previous publication to realize the confinement geometry of coil−coil block copolymers.[12,37] The main idea of this method is that a surface density field, $\phi_W(\mathbf{r})$ (W stands for the walls, $0 \le \phi_W(\mathbf{r}) \le 1$), is introduced to confine the system into the enclosed region between two parallel surfaces. The polymers are expelled by imposing an incompressibility constraint, namely, $\phi_R(\mathbf{r}) + \phi_C(\mathbf{r}) + \phi_W(\mathbf{r}) = 1$, where $\phi_R(\mathbf{r})$ and $\phi_C(\mathbf{r})$ denote normalized segment density fields for rod and coil species, respectively. Therefore, the choice of $\phi_W(\mathbf{r})$ determines the geometry of the films and here we consider the two parallel walls normal to the z-axis with a hyperbolic tangent functional form:

$$\phi_W(z) = \frac{1}{2}\left\{1 - \tanh\left[\frac{m}{t}\left(\frac{1}{2}(L_z - T) - \left|z - \frac{1}{2}L_z\right|\right)\right]\right\} \tag{5}$$

where the parameter T represents the range of a wall interaction along position z and m and t are factors used to define the transition region and to set the width of the transition region from the wall to the polymers, respectively (see our previous paper for details[12,37]). The value of interfacial thickness of the transition t is fixed as $0.3R_g$ and the value of T is fixed as $1.25R_g$. Thus the effective thickness of the confinement system is $D = L_z - T$ and the effective volume occupied by copolymers is modified to $V = \int d\mathbf{r}\,(1 - \phi_W(\mathbf{r}))$. The confining wall is modeled as a fixed density field that interacts with the polymer segments via the incompressibility constraint and Flory−Huggins interactions. Furthermore, we can consider SCFT model of the RC DBC in bulk as a special case with $\phi_W(\mathbf{r}) = 0$ in the XZ-plane.

The above interactions can be dealt with energy penalties ascribed to the spatial variations of the order parameters such as distributions of the densities of rods and coils and orientational order of rod blocks. Therefore, the free energy functional in the unit of nk_BT of RC DBC is

$$\begin{aligned} F = \frac{1}{V}\int d\mathbf{r}\,[&\chi N\phi_R(\mathbf{r})\,\phi_C(\mathbf{r}) + \chi_{CW}N\phi_W(\mathbf{r})(1 - \phi_W(\mathbf{r})) + \\ &(\chi_{RW}N - \chi_{CW}N)\phi_R(\mathbf{r})\,\phi_W(\mathbf{r}) - \omega_C(\mathbf{r})\,\phi_C(\mathbf{r}) - \omega_R(\mathbf{r})\,\phi_R(\mathbf{r}) + \\ &\eta(\mathbf{r})\Big(\sum_P \phi_P(\mathbf{r}) - 1\Big) - \frac{\mu N}{2}\mathbf{T}(\mathbf{r}):\mathbf{T}(\mathbf{r}) + \mathbf{M}(\mathbf{r}):\mathbf{T}(\mathbf{r})] - \ln Q \end{aligned} \tag{6}$$

where χ is the Flory−Huggins interaction parameter between unlike rod and coil segments, which favors their microphase separation and χ_{PW} is a dimensionless measure of the surface energy between species (P = R, C) and the walls. $\eta(\mathbf{r})$ ensures the incompressibility of the system. $\mathbf{T}(\mathbf{r})$ is a normalized orientational order parameter field. Orientational interactions are described by a Maier−Saupe interaction energy in the mean-field framework, where μ denotes the strength of the orientation interactions favoring the parallel alignment of rod blocks.[38] Q is the single chain partition function in the external fields:

$$Q = \frac{1}{V\int d\mathbf{u}}\int d\mathbf{u}\int d\mathbf{r}\,\exp\left[-\int_0^{1-f} ds\,\Gamma(\mathbf{r} + \beta s\mathbf{u},\mathbf{u})\right] q(\mathbf{r},f) \tag{7}$$

According to the mean-field approximation, the following SCFT equations for RC DBC are obtained by minimizing the free energy functional eq 5 with respect to $\phi_P(\mathbf{r})$, $\omega_P(\mathbf{r})$, $\mathbf{T}(\mathbf{r})$, $\mathbf{M}(\mathbf{r})$, and $\eta(\mathbf{r})$:

$$\omega_C(\mathbf{r}) = \chi N\phi_R(\mathbf{r}) + \chi_{CW}N\phi_W(\mathbf{r}) + \eta(\mathbf{r}) \tag{8}$$

$$\omega_R(\mathbf{r}) = \chi N\phi_C(\mathbf{r}) + \chi_{RW}N\phi_W(\mathbf{r}) + \eta(\mathbf{r}) \tag{9}$$

$$\phi_R(\mathbf{r}) + \phi_C(\mathbf{r}) + \phi_W(\mathbf{r}) = 1 \tag{10}$$

$$\phi_C(\mathbf{r}) = \frac{1}{Q}\int_0^f ds\, q(\mathbf{r},s)\, q^*(\mathbf{r},s) \tag{11}$$

$$\phi_R(\mathbf{r}) = \frac{1}{Q\int d\mathbf{u}}\int_0^{1-f} ds \int d\mathbf{u}\, q(\mathbf{r}-\beta s\mathbf{u},f) \times \exp\left[-\int_0^{1-f} ds'\,\Gamma(\mathbf{r}-\beta\mathbf{u}(s-s'),\mathbf{u})\right] \tag{12}$$

$$\mathbf{M}(\mathbf{r}) = \mu N\mathbf{T}(\mathbf{r}) \tag{13}$$

$$\mathbf{T}(\mathbf{r}) = \frac{1}{Q\int d\mathbf{u}}\int_0^{1-f} ds \int d\mathbf{u}\, q(\mathbf{r}-\beta s\mathbf{u},f) \times \exp\left[-\int_0^{1-f} ds'\,\Gamma(\mathbf{r}-\beta\mathbf{u}(s-s'),\mathbf{u})\right]\left(\mathbf{uu} - \frac{\mathbf{I}}{3}\right) \tag{14}$$

Equations 8−14 form a closed set of self-consistent equations, which can be numerically implemented by combinatorial screening algorithm proposed by Drolet and Fredrickson.[14] In addition, the diffusion eqs 1 and 2 is solved to obtain $q(\mathbf{r},s)$ and $q^*(\mathbf{r},s)$ with the pseudospectral operator splitting algorithm, which can be readily implemented by fast Fourier transforms.[39] In this work, the simulations are carried out on a 2D position space (XZ-plane) with $L_x \times L_z$ lattice points with periodic boundary conditions in x- and z-directions. The grid size of the space is chosen as $\Delta x = \Delta z = 0.125R_g$. The discretization of contour variable s is chosen to be $\Delta s = 0.01$ and $\Delta s = 0.05$ for coil segments and rod segments, respectively. However, the orientation of rods is still in 3D space, and the angular quadrature is still performed over an arbitrary unit vector $\mathbf{u}$ on the spherical surface. With the help of our previous paper,[33] the spherical surface is discretized into icosahedron triangular mesh with $M = 1442$ vertexes to ensure the accurate discretization of the angle distribution of rods. To obtain the relatively stable morphologies of RC DBC, we start the performance of the calculation with both random initial orientation fields and completely aligned angle ranging from 0 to $\pi/2$ by a step of $\pi/12$ along z-axis, but with random initial composition fields in each case. Moreover, for a given film thickness D, we minimize the free energy F with respect to L_x to minimize the influence of the simulation box sizes in x-direction, each minimization of the free energy is iterated with respect to L_x (integer multiples of the confined period in x-direction) by a step of $0.25R_g$. The final stable phase structure is thus determined as the one having the lowest free energy. Furthermore, the pseudodynamical evolutions[15] are carried out to a convergence of 10^{-5} in free energy and a convergence of 10^{-4} in fields values.

Results and Discussion

As a test case of our numerical algorithm, we first demonstrate the influence of numerical accuracy of solving SCFT equations

on the bulk phase behavior of RC DBC ($\phi_W(\mathbf{r}) = 0$ in the XZ-plane). The size asymmetry ratio $\beta = Nb/(a^2N/6)^{1/2} = 6^{1/2}\nu^{-1}$ and the parameter μN controlling the strength of the rod interactions are chosen to be identical to those used by Pryamitsyn and Ganesan[24] for comparison, i.e., $\nu = 0.15$ ($\nu = 0.25$) and $G = \mu/\chi = 4$ with varying χN. We then focus on the self-assembly of RC DBC confined between two identical flat walls. For the sake of simplicity, we consider two cases: rod monolayer smectic-C in bulk formed in the case of $f = 0.4$ and $\nu = 0.5$, and hockey puck-shaped phase in bulk formed in the case of $f = 0.6$ and $\nu = 0.25$. From the free energy functional eq 6, we see that the interactions between the walls and the two blocks depend only on the difference between $\chi_{RW}N$ and $\chi_{CW}N$, namely, $\Delta\chi_{PW}N = \chi_{RW}N - \chi_{CW}N$. We therefore fix $\chi_{CW}N$ to be 0 throughout our simulations. Two surface conditions are considered here: neutral ($\Delta\chi_{PW}N = 0$) and attractive for the rods ($\Delta\chi_{PW}N < 0$). For neutral walls, we investigate the effects of D, the orientational interaction between rod blocks μN and the Flory−Huggins interaction between rod and coil segments χN on the morphologies of confined rod−coil copolymers. For rod-attractive walls, we consider the phase transition under different strength of the interactions between the surfaces and copolymers and investigate the effects of the surface field on the phase behavior of RC DBC with different size asymmetry ratio β.

A. Bulk Results. In eqs 3, 7, 12, and 14, the integration of the functions defined on a unit spherical surface $\int f(\mathbf{u})\, d\mathbf{u}$ needs to be evaluated. Pryamitsyn and Ganesan[24] calculated these integrals using a 10-point Gaussian quadrature for θ and a 20-point Gaussian quadrature for ϕ, where $\theta \in [0, \pi]$ and $\phi \in [0, 2\pi)$ refer to the angles in spherical coordinates. As pointed out by them, the use of a coarse discretization for these angles is probably the most error-prone part in their SCFT calculations.[24] Our calculations also show that finding the equilibrium structure is somewhat difficult because the space dimensions have to be commensurate with the tilting angle of the rods and the bulk period of the self-assembled structures, which requires finer and more accurate discretization of rod orientation. In this work, the unit-sphere surface is spatially discretized with nearly uniform icosahedron triangular lattice of M vertices (see our previous paper[33] for details). A vertex on the unit sphere can be represented as a unit vector in Cartesian coordinates: $\mathbf{u}[M] = (u_{mx}, u_{my}, u_{mz}) \in R^3$, $|\mathbf{u}[M]| = 1$. The angular quadrature of a function can then be numerically evaluated as the sum of the function values multiplied by the corresponding Voronoi cell area at these vertices. For example, $q^*(\mathbf{r},s=f)$ in eq 3 can be expressed as

$$q^*(\mathbf{r},s=f) = \frac{\sum_M A_M \exp[-\int_0^{1-f} ds\, \Gamma(\mathbf{r} + \beta s\mathbf{u}[M],\mathbf{u}[M])]}{\sum_M A_M} \tag{15}$$

where A_M is the area of one-ring Voronoi region at each vertex.

We have repeated the 2D calculation phase diagram by Pryamitsyn and Ganesan,[24] as a function of f and χN for $\nu = 0.15$ and $\nu = 0.25$, and the results show that most morphologies obtained using our numerical quadrature method are consistent with their work, including smectic-A, smectic-C, puck-shaped phases, and broken lamellae. Our nearly uniform triangular mesh discretization, however, describes the rod orientations in 3D Euclidean space more accurately, thus leading to more accurate angular quadrature. Furthermore, the adopted $M = 1442$ vertex points for the discretization of the rod orientation ensure that the convergence of both free energy and fields are at least an order of magnitude increased compared to the Gaussian quadrature. Here we illustrate the numerical stability and accuracy of our method in the case of $f = 0.35$, $\chi N = 8$, $G = 4$, and $\nu = 0.25$.

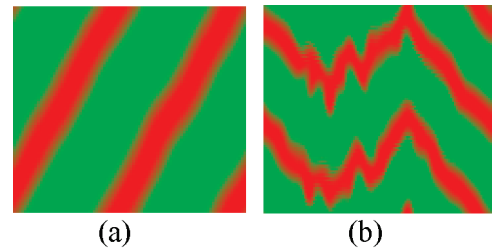

Figure 1. Self-assembly of RC DBC for $f = 0.35$, $\chi N = 8$, $G = 4$, and $\nu = 0.25$. The red and green colors represent the coil and rod blocks, respectively. (a) Rod monolayer smectic-C (mC) phase with icosahedron triangular mesh discretization on the sphere employed to calculate angular integral in our simulations. (b) Nonequilibrium chevronlike structure with normal Gaussian quadrature to numerically solve the rod orientational integration of the functions defined on a unit spherical surface.

Figure 1 shows self-assembled morphologies of RC DBC performed by different numerical quadratures for rod orientations. The rod monolayer smectic-C (noted as mC) phase shown in Figure 1a obtained with our icosahedron triangular mesh quadrature is found to be stable with the lowest free energy per chain F over all other structures with varying different initial guesses of the rods alignment and box sizes. In contrast, the nonequilibrium chevron structure shown in Figure 1b is obtained by Pryamitsyn and Ganesan,[24] as well as in our simulations, with the Gaussian quadrature. We attribute this discrepancy to the problem of lower accuracy due to coarse discretization of orientational angles in Gaussian quadrature technique used for angular integrals. In fact, well ordered periodic morphologies are not easy to obtain when the intensity of rod interactions is relatively strong with the pseudodynamical evolutions of the SCFT equations, especially when a coarser discretization for the orientational angles is adopted.

The microstructure of the mC phase in Figure 1a is determined by the segmental density profiles and the orientation order parameters of rods. According to SCFT, the density distribution $\varphi(\mathbf{r},s)$ of the sth segment of the rod block at position $\mathbf{r}$ is given by

$$\varphi(\mathbf{r},s) = \frac{\int d\mathbf{u}\, q(\mathbf{r}-\beta s\mathbf{u},f) \exp[-\int_0^{1-f} ds'\, \Gamma(\mathbf{r}-\beta\mathbf{u}(s-s'),\mathbf{u})]}{Q \int d\mathbf{u}} \tag{16}$$

Furthermore, the degree of the rod alignment is quantified by an order parameter: $\tilde{T}(\mathbf{r}) = 3/2 \times \gamma_{max}(\mathbf{r})$, where $\gamma_{max}(\mathbf{r})$ is the maximum eigenvalue and $\mathbf{\Lambda}(\mathbf{r}) = [\Lambda_x(\mathbf{r}) \quad \Lambda_y(\mathbf{r}) \quad \Lambda_z(\mathbf{r})]^T$ is the corresponding eigenvector (representing the main orientation of the rods) of the orientational tensor $\mathbf{T}(\mathbf{r})$.[24] $\tilde{T}(\mathbf{r}) = 1$ denotes complete alignment of rods and its deviation from unity quantifies the disalignment degree of the rods. We note that we only consider $\tilde{T}(\mathbf{r})$ and $\mathbf{\Lambda}(\mathbf{r})$ at $\mathbf{r}$ of maximum rod density. Figure 2a shows the density distribution of coil segments $\phi_C(l)$, rod segments $\phi_R(l)$, rod terminals $\varphi(l,s=1)$ and the rod−coil junctions $\varphi(l,s=f)$ as a function of position l along the lamellar normal $\mathbf{n}$. The average tilting angle of rods Θ with respect to

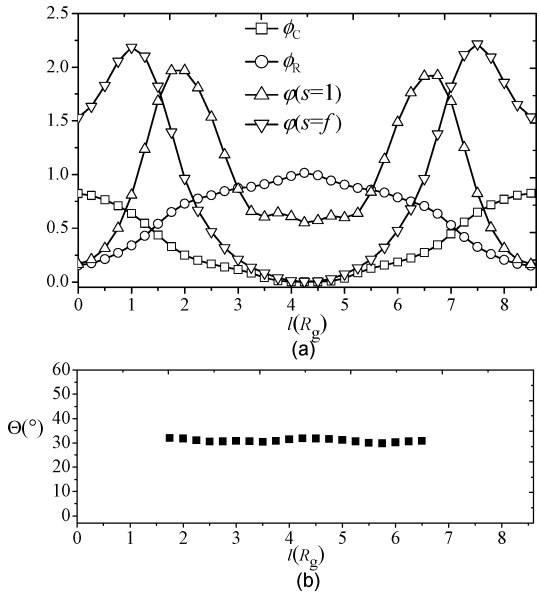

Figure 2. (a) Density profiles of coils $\phi_C(l)$, rods $\phi_R(l)$, the segment of rod terminals $\varphi(l,s=1,)$ and the rod−coil junctions $\varphi(l,s=f)$ with the axis l along the lamellar normal **n** for the mC phase in Figure 1a. (b) Averaged tilting angle of rods with respect to lamellar normal **n** $\Theta(l)$ along l. Θ is considered only in the rod rich domain $\phi_R(l) > (1 - f)$.

the lamellar normal **n** as a function of l is plotted in Figure 2b. From Figure 2a, the coils are almost completely expelled from the middle of the rod domain. Accordingly, Θ is almost constant ($\Theta \approx 30-32°$) in the rod-rich region in Figure 2b. Moreover, the rod alignment $\tilde{T}$ is relatively large, $\tilde{T} = 0.91$, indicating that the rods are well oriented by the Maier−Saupe orientational interactions between rods. From Figure 2a, the density of the rod terminals $\varphi(l,s=1)$ exhibits two peaks over the bulk lamellar period of $L_b \approx 8.5R_g$, which are very close to the two maxima of the rod−coil junctions $\varphi(l,s=f)$. Since the rod length is $(1 - f) \times \beta = 6.37R_g$ and $\Theta \approx 31°$, the projected length of a rod block onto the lamellar normal is about $6.37R_g \times \cos 31° = 5.46R_g$. This is larger than the distance between the two peaks of rod terminals (about $4.75R_g$), showing a high degree of interdigitation of parallel rod blocks. Therefore, this structure in Figure 1a is denoted as a rod monolayer smectic-C phase (mC). In this case, the occurrence of the smectic-C can be attributed to the fact that stronger Maier−Saupe orientation interaction favors more closely packed and well-aligned rods, simultaneously reducing rod−coil interfacial energy. On the other hand, stronger rod packing leads to a smaller interfacial area per chain, thus increasing the stretching energy of the coils. To reduce the stretching energy of coils, the rods tilt by an angle to the lamellae normal, forming a smectic-C phase while sacrificing the less important (at this conditions of less strong microphase separation) interfacial energy. Therefore, the existence of the smectic-C is a result of the competitive effects between rod−coil interfacial energy and coil−stretching energy due to orientational interactions for rods.[17,40] For the same reason with the decrease in ν parameter (small ν corresponds to small rod diameter leading to large stretching energy penalty of coils), the coil−stretching energy dominates, thus leading to smectic-C structure, as mentioned by Matsen and Barrett.[17]

Considering the smectic-C phase under confinement, we consider more weakly segregated RC DBC with $f = 0.4$, $\chi N = 6$, $\mu N = 24$, and $\nu = 0.5$ in contrast to Figure 1a, which forms a rod monolayer smectic-C phase (mC) similar to that in Figure 1a. We note that higher values of ν are chosen for saving

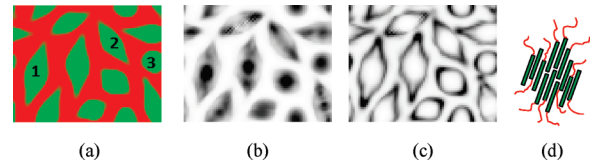

Figure 3. (a) Rod puck-shaped phases in RC DBC for $f = 0.6$, $\chi N = 13$, $G = 4$, and $\nu = 0.25$ with randomly initial orientation fields. The red and green colors represent the coil and rod blocks, respectively. (b) and (c) show density distributions of the rod terminals $\varphi(l,s=1)$ and rod−coil junctions $\varphi(l,s=f)$ corresponding to (a), respectively. (d) Schematic model of the puck-shaped phase corresponding to rod domain 1 in (a).

computational loads. However, the tilting angle of rods to the lamellar normal is $\Theta \approx 20°$, the degree of rod alignment $\tilde{T} = 0.80$, and the lamellar period of $L_b \approx 5.25R_g$. Furthermore, we consider the following cases: (1) only increase the orientation interactions between rods, i.e., μN increased from $\mu N = 24$ to $\mu N = 36$; (2) increase the repulsion between rod and coil segments, i.e., χN increased from $\chi N = 6$ to $\chi N = 10$ but with fixed $\mu N = 24$; (3) increase χN but decrease μN, i.e., $\chi N = 12$ and $\mu N = 12$. The mC phase is found in bulk for all the three cases, with $\tilde{T} = 0.911$ and $L_b \approx 5.37R_g$ for case (1), $\tilde{T} = 0.888$ and $L_b \approx 5.5R_g$ for (2), and $\tilde{T} = 0.52$ and $L_b \approx 4.9R_g$ for (3). In cases (1) and (2), $\tilde{T}$ is increased with the increasing orientational interactions between rods or Flory−Huggins interactions between rods and coils, although the two interactions provide different contributions to the free energies. Flory−Huggins repulsion between the two species can lead to the microphase separation of the RC DBC, further promoting the alignment of the rods. At the same time, the orientational interactions between rods can also promote the microphase separation of the RC DBC even with $\chi N = 0$ as long as μN is large enough, such as $\mu N \geq 40$ in our simulations. However, in the case of $\chi N = 12$ and $\mu N = 12$, the degree of rods alignment is low ($\tilde{T} = 0.52$), indicating that when μN is not strong enough, good alignment of rods is difficult to be obtained even if microphase separation happens.

In addition to the mC phase, we also obtain the hockey puck-shaped phase at $f = 0.6$, $\chi N = 13$, $G = 4$, and $\nu = 0.25$, shown in Figure 3a. This phase is similar to that obtained by Pryamitsyn and Ganesan[24] with the Gaussian quadrature. In this case, the majority component coil blocks can fan out into larger region of space, hence stretching less while inducing the interfacial energy penalty (stretching energy is proportional to the volume fraction of coils). We further compute $\tilde{T}$ in three different rod domains denoted as 1, 2, and 3 in Figure 3a, and obtain $\tilde{T} = 0.93$, 0.93, and 0.915, respectively, all indicating almost complete rod alignment in the hockey puck-shaped phase. We also obtain the main orientation of rods, i.e., eigenvector $\mathbf{\Lambda}$: $\mathbf{\Lambda} = [0.347 \quad 0.009 \quad -0.938]^T$, $\mathbf{\Lambda} = [0.570 \quad 0.049 \quad 0.820]^T$, and $\mathbf{\Lambda} = [0.493 \quad 0.870 \quad 0.016]^T$ for the rod domains 1, 2, and 3, respectively. The results show that the rods in domain 1 have relatively large values of the x-component Λ_x and z-component Λ_z but with quite small values of $\Lambda_y = 0.009$, indicating the orientation of rods lies in the XZ-plane. The rods in domain 2 orient nearly in the XZ-plane with $\Lambda_y = 0.049$, similar to the case in domain 1. However, the values of Λ_x and Λ_y in rod domain 3 are relatively large but with a small value of Λ_z, indicating the rods orient nearly in the XY-plane, which is different from rods in domains 1 and 2. We therefore conjecture that the puck-shaped structures are randomly oriented in the system but with good alignment in each rod domain.

To further investigate the puck-shaped structure of the self-assembled RC DBC, the density distribution of rod terminals

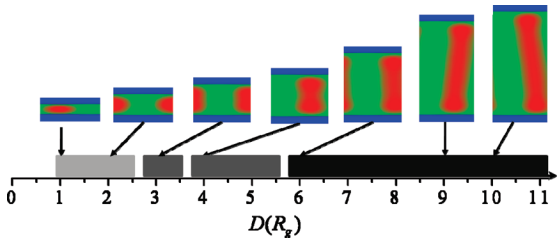

Figure 4. Representative 2D microstructures of weakly segregated mC phase formed in the case of $f = 0.4$, $\chi N = 6$, $G = 4$, and $\nu = 0.5$, under confinement for neutral walls ($\Delta\chi_{PW}N = 0$) as a function of thickness D. The rectangle area denotes the region occupied by the arrow pointed structure, corresponding to arrow pointed film thickness. For simplicity, only one confined lamellar period are shown here. The red, green and blue colors represent the coils, rods, and flat surfaces, respectively.

$\varphi(l,s=1)$ and the rod−coil junctions $\varphi(l,s=f)$ are displayed in Figure 3b,c respectively, corresponding to Figure 3a. From Figure 3b,c, we propose that the arrangement of RC DBC in puck-shaped phase is a combination of smectic-C bilayers and monolayer structure. We illuminate the structure of rod domain 1 in Figure 3a as an example. In domain 1, the observed size along the long axis parallel to rod orientation of the puck-shaped phase, denoted as l_a, is about $8.25R_g$, which is almost twice the rod length $2 \times (1 - f) \times \beta = 7.84R_g$ and the size of the short axis denoted as l_b is about $3.0R_g$. The high density distribution of the rod terminals in the center of the puck-shaped phase in Figure 3b indicates rod bilayer smectic structure, favoring rod−coil interfacial energy. Furthermore, from Figure 3c, relatively higher density distribution of rod−coil junctions at the two ends along the long axis than that at the other rim of puck-shaped structures proves the combination of bilayer in the center and other monolayer smectic structures. Therefore, we propose the combination of smectic-C bilayers and monolayer phases corresponding to rod domain 1 shown in Figure 3d, like the suggested model by Pryamitsyn and Ganesan.[24]

B. Thin Films Between Neutral Walls. In this section, we consider thin films of RC DBC with two coil volume fractions: $f = 0.4$ and $f = 0.6$, where the rod monolayer smectic-C phase and rod puck-shaped phase form in bulk, as discussed above. In such thin films, the most stable phase is determined by the balance among the Flory−Huggins interaction favoring microphase separation between rods and coils, the elastic free-energy penalty for coil−stretching at the rod−coil interfaces (the sharper the interface, the larger the coil−stretching) and near the film surfaces, rod−coil interfacial energy, and orientational interactions between rods favoring their alignment.

Layered Smectic-C Phase under Confinement. We first consider weakly microphase-segregated RC DBC with $f = 0.4$, $\chi N = 6$, $G = 4$, and $\nu = 0.5$, which form a rod monolayer smectic-C phase (mC) similar to that in Figure 1a but with $\Theta \approx 20°$, $\tilde{T} = 0.80$, and $L_b \approx 5.25R_g$, as discussed above. Figure 4 shows the corresponding thin-film morphologies formed under confinement between two neutral walls as a function of D. At all D, we see a thin rod layer near each surface due to the strong conformational asymmetry between rod and coil blocks: Coil blocks lose much more conformational entropy near an impenetrable surface than rigid rods and are thus depleted from the surface. An energetically neutral and impenetrable surface therefore exhibits entropic preference for rod blocks. This is closely related to the phenomenon in experiments that the rod layers are particularly well developed near the surfaces of the film.[41] In particular, for confined coil−coil copolymer melts with symmetric composition, lamellae perpendicular to the nonpreferential surfaces are always stable,[9,42] although the enrichment of chain ends and depletion of middle segments near the surfaces favor parallel morphologies due to the hard-surface effect.[43] In our simulations, for the mC phase formed in bulk, lamellae always orient perpendicular to the surfaces (i.e., $L^{\perp}$) with a lower free energy compared with the those of parallel lamellae (i.e., $L^{\parallel}$) regardless of the film thickness, as shown in Figure 4. This observation is in accordance with experimental[13,41] and theoretical studies.[25] In thin films, perpendicular lamellae can relax to the bulk spacing, while the parallel lamellae cost energy for the largely coil−stretching. However, in the case of $\chi N = 12$ and $\mu N = 12$ under confinement, $L^{\parallel}$ appears at $D = 5.5R_g$ (figures not shown here), comparable to the bulk lamellar period of $L_b \approx 4.9R_g$. With a low degree of rod alignment in bulk $\tilde{T} = 0.52$, the coil−stretching in the thin film is not strong; therefore, the energetically neutral and impenetrable surface exhibits entropic preference for rod blocks, leading to form $L^{\parallel}$.

According to eq 6, the mean-field free energy per chain $F = F_{el} + F_{RC} + F_{M-S} + F_{sf}$ consists of the elastic energy mainly associated with coil−stretching entropy

$$F_{el} = \frac{1}{V}\int d\mathbf{r}\,[-\omega_C(\mathbf{r})\,\phi_C(\mathbf{r}) - \omega_R(\mathbf{r})\,\phi_R(\mathbf{r})] - \ln Q$$

rod−coil interfacial energy

$$F_{RC} = \frac{1}{V}\int d\mathbf{r}\,\chi N\phi_R(\mathbf{r})\,\phi_C(\mathbf{r})$$

Maier−Saupe orientational interaction favoring the parallel alignment of rod blocks

$$F_{M-S} = \frac{1}{V}\int d\mathbf{r}\left[-\frac{\mu N}{2}\mathbf{T}(\mathbf{r}):\mathbf{T}(\mathbf{r}) + \mathbf{M}(\mathbf{r}):\mathbf{T}(\mathbf{r})\right]$$

and the surface energy

$$F_{sf} = \frac{1}{V}\int d\mathbf{r}\,[\chi_{CW}N\phi_W(\mathbf{r})(1 - \phi_W(\mathbf{r})) + (\chi_{RW}N - \chi_{CW}N)\phi_R(\mathbf{r})\,\phi_W(\mathbf{r})]$$

The stability of various phases is determined by the balance among F_{el}, F_{RC}, F_{M-S}, and F_{sf} (for netral walls, $F_{sf} = 0$). Figure 5 shows the free energy and its components for the morphologies ($L^{\perp}$) in Figure 4. When $D < 4R_g$, the free energy is mainly driven by coil−stretching energy F_{el}. When the film is very thin, such as $D = 1R_g$, the coils are strongly stretched. To reduce the coil−stretching, the rod−coil interface is curved and the spindle-shaped structures of coils in Figure 4 occur. With the increasing of D, F_{el} decreases and thus the curved degree of the interface decreases. When D is increased to $D = 3R_g$, the curved interface nearly disappears and $L^{\perp}$ phases are obtained instead. With further increasing D, the confinement effect on the microstructures of copolymers in the center of the film reduces, thus forming $L^{\perp}$ with dumbbell-shaped coil domains in the case of $D = 4-5.5R_g$. In particular, $L^{\perp}$ phases slightly tilt along the surfaces, especially when $D \geq 6R_g$, and the value of the tilting angle increases from $D = 6R_g$ to $D = 10R_g$ because large enough space between two surfaces allows the lamellae to relax to the smectic-C phase in bulk. Simultaneously, the rods tend to align along the x-axis (horizontal direction) and the lamellae arrange titled to the surfaces. Furthermore, the effect of film thickness

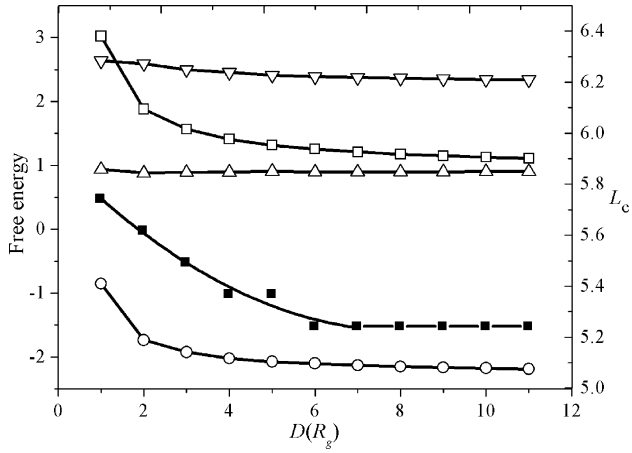

Figure 5. Mean-field free energy per chain F (□) consisting of coil−stretching entropy F_{el} (○), rod−coil interfacial energy F_{RC} (Δ), and Maier−Saupe orientational interaction F_{M-S} (▽) for perpendicular lamellae in Figure 4 (where the surface energy $F_{sf} = 0$ for neutral walls). The domain spacing L_c of perpendicular lamellae under confinement (■) in Figure 4 with bulk lamellar period of $L_b = 5.25R_g$.

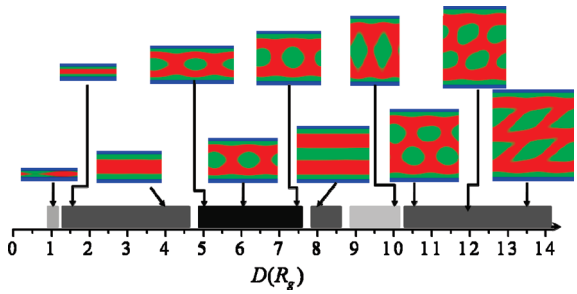

Figure 6. Representative 2D microstructures of the bulk puck-shaped phase in Figure 3 under confinement into neutral walls ($\Delta\chi_{PW}N = 0$) with varying film thickness D. The rectangle area denotes the region occupied by the arrow pointed phase, corresponding to arrow pointed film thickness. Red, green, and blue represent the coils, rods, and flat surfaces, respectively.

D, i.e., confinement on the confined lamellar period L_c, is also shown in Figure 5. When $D = 1R_g$, $L_c = 5.75R_g$, which is larger than bulk period $L_b = 5.25R_g$. Then L_c decreases to L_b with increasing $D \geq 6R_g$. This agrees with the experimental findings[7] that the extent of dilation of the lamellar domain spacing in thin films decays exponentially to the bulk domain spacing with increasing film thickness.

We use $\tilde{T}_{sur}$ to denote the degree of the rod alignment in the rod domains near the surfaces, and $\tilde{T}_{int}$ denotes that in the center of the film. For D within $2-5.5R_g$, $\tilde{T}_{sur} = 0.84$, which is larger than that in bulk ($\tilde{T} = 0.80$). The well-aligned rods near the surface also leads to a higher degree of the internal rods alignment, i.e., $\tilde{T}_{int} \approx 0.82$. When $D > 5.5R_g$, which is close to L_b, $\tilde{T}_{int} \approx 0.80$, almost the same as the value in bulk. This is confirmed in Figure 5 where rod orientational interaction energy F_{M-S} decreases as D increases from $1R_g$ to $6R_g$ while keeping constant for $D > 6R_g$. In this case, the effect of the geometrical confinement is thus weakened with increasing film thickness, similar to the experimental situation.[7]

Hockey Puck-Shaped Phase under Confinement. Here we take $f = 0.6$, $\chi N = 13$, $\mu N = 52$, and $\nu = 0.25$, where the puck-shaped phase is stable in bulk, as shown in Figure 3a. Figure 6 shows the corresponding thin-film morphologies confined between two neutral surfaces as a function of D. Like confined layered smectic-C phase in Figure 4, we again see a thin layer of rods near each surface with orientation lying in

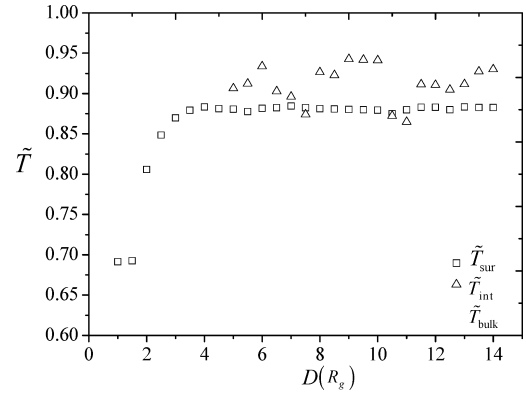

Figure 7. Order parameter $\tilde{T}$ for the puck-shaped phases under confinement corresponding to the phase diagram in Figure 6. $\tilde{T}_{sur}$ and $\tilde{T}_{int}$ represent the averaged order parameter of the rods near the surfaces and in the interior, respectively.

the XY-plane at all D due to the entropic preference of the impenetrable surfaces for rod blocks. In the interior of the film, we find parallel lamellae $L^{\parallel}_i$, where $i = 1, 2, 3$ denotes the number of rod layers, and puck-shaped phase alternating with increasing D from $1R_g$ to $14R_g$ by a step of $0.5R_g$.

The degree of rod alignment in the rod domains near the surfaces $\tilde{T}_{sur}$ and in the interior of the film $\tilde{T}_{int}$ of the puck-shaped phase under confinement as a function of D are plotted in Figure 7. When the film is very thin (i.e., $D = 1R_g$), the spindle-shaped structure of coils as shown in Figure 6 (similar to the case of confined mC phase in Figure 4) forms to reduce coil−stretching F_{el} in such a narrow space, while inducing a relatively large rod−coil interfacial area (large rod−coil interfacial energy F_{RC}). In this case, the value of $\tilde{T}_{sur}$ is relatively low, as shown in Figure 7. For $D = 1.5R_g$, parallel lamellae $L^{\parallel}_2$ are found, while the rod−coil interfacial area is large to relax the highly stretched coils, resulting in low degree of rod alignment $\tilde{T}_{sur} = 0.69$. With further increasing D, F_{el} decreases and $\tilde{T}_{sur}$ increases from 0.69 to 0.88 with rods oriented parallel to surfaces when D is increased from $1.5R_g$ to $4R_g$. For $D = 4-14R_g$, $\tilde{T}_{sur}$ levels off at a value slightly smaller than that in bulk $\tilde{T} = 0.93$ due to confined surfaces. We also note that, for $D = 5-14R_g$, the thickness of the rod layer near each surface remains constant (about $0.7R_g$) with rods oriented parallel to the surfaces.

For $D \geq 5R_g$, the puck-shaped phase emerges in the interior of the film in favor of reducing the coil−stretching energy. In the case of $D = 5R_g$, the eigenvector describing the main orientation of the rods is $\mathbf{\Lambda} = [0.143 \quad -0.990 \quad 0]^T$, indicating that the orientation of puck-shaped phases lies in the XY-plane with the z-component $\Lambda_z = 0$ and mainly oriented along the y-axis. Furthermore, the rod alignment in puck-shaped domains $\tilde{T}_{int} = 0.905$ is still lower than that in bulk, because the maximum length of confined puck-shaped phase $l_c \approx 2.1R_g$ along film thickness is not commensurate with the bulk size $l_a \approx 8.25R_g$ and $l_b \approx 3.0R_g$. This similarly occurs in the case of $D = 7 - 7.5R_g$ and $D = 10.5-12.5R_g$ with lower $\tilde{T}_{int}$ than that in bulk because l_c is not commensurate with l_a. However, at $D = 6R_g$, l_c is about $2.8R_g$, comparable to l_b in bulk; the degree of rod alignment is therefore relatively large, such as $\tilde{T}_{int} = 0.934$. And $\mathbf{\Lambda} = [-0.589 \quad -0.808 \quad 0.012]^T$, indicating that the orientation of the rods mainly lies in the XY-plane with a small value of Λz. Interestingly, in the case of $D = 9-10R_g$, slightly larger than $l_a = 8.25R_g$ in bulk, the completely upright puck-shaped phase is obtained with a high rod alignment $\tilde{T}_{int} = 0.94$, close to that in bulk.

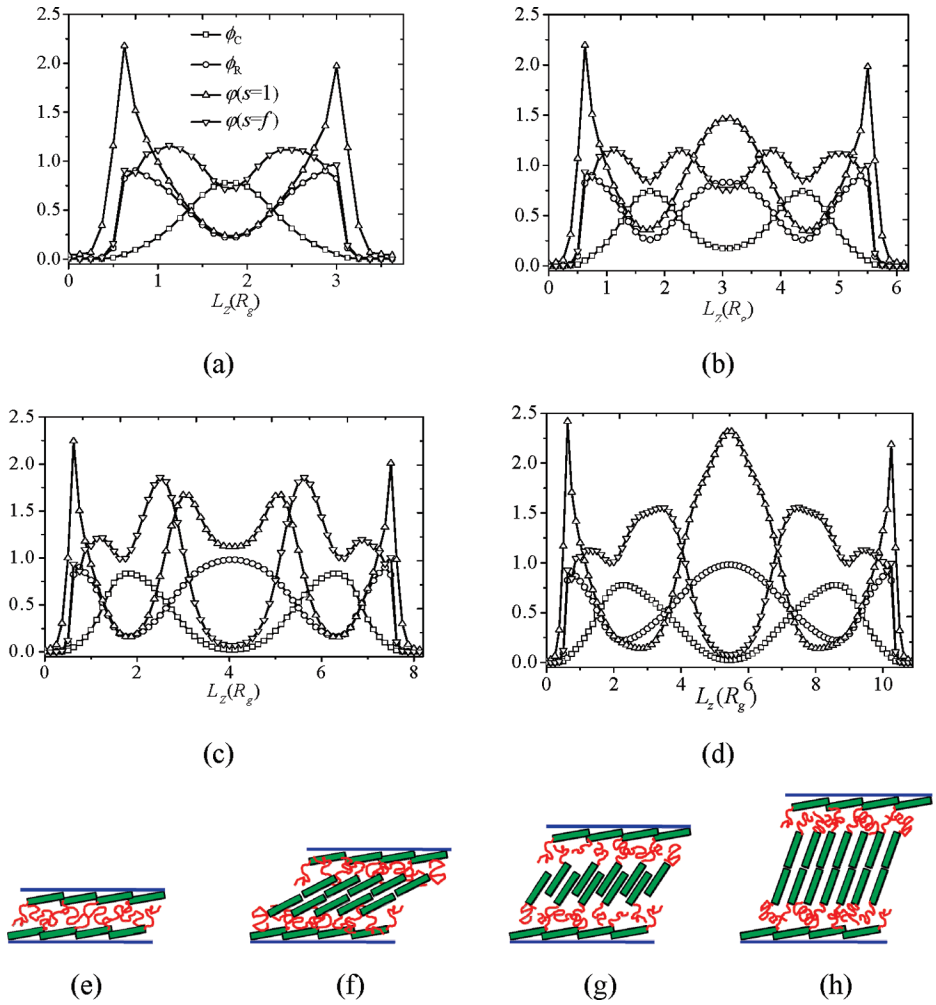

Figure 8. Density profiles for rod smectic-C phase formed in $f = 0.4$, $\chi N = 6$, $G = 4$, and $\nu = 0.5$ for $\Delta\chi_{PW}N = -35$ with varying film thickness D: (a) $D = 2.5R_g = 0.48L_b$; (b) $D = 5R_g = 0.95L_b$; (c) $D = 7R_g = 1.33L_b$; (d) $D = 9.75R_g = 1.85L_b$. (e)−(h) represent schematic smectic-C phases $L^{\parallel}$, bC $L^{\parallel}$, mC $L^{\parallel}$, and bC $L^{\parallel}$, corresponding to the density profiles of the confined rod−coil systems (a)−(d), respectively.

In addition, in the case of $D = 8-8.5R_g$, parallel lamellae $L^{\parallel}_3$ with the orientation of rods lying in the XY-plane are obtained as the transition structure between the rod puck-shaped phase with rod orientation lying in the XY-plane at $D = 7.5R_g$ and that with rods aligned perpendicular to the surfaces at $D = 9R_g$. In this case, the rod−coil interface is quite sharp with a high degree of rod alignment, $\tilde{T}_{int} = 0.925$, and the middle rod layer is a rod bilayer smectic-C phase denoted as bC with the average tilting angle of rods Θ to the lamellar normal of about 70°. When D is large enough, such as $D = 13-14R_g$, the confinement effect on the self-assembled morphologies of RC DBC is not significant and the microstructures and $\tilde{T}_{int}$ are almost the same as those in bulk. Finally, we note that for all the puck-shaped structures shown in Figure 6, in contrast to the random orientation for different puck-shaped structures obtained in bulk, the rods are oriented in the same direction for all rod puck-shaped structures under confinement.

C. Thin Films between Rod-Attractive Walls. Besides lamellae perpendicular to the surfaces $L^{\perp}$, the parallel lamellae $L^{\parallel}$ have also been investigated in experements.[6,7] To obtain lamellae oriented parallel to the surfaces, the surfaces have to energetically prefer either rod or coil blocks. Due to the entropic preference of the surfaces for the rod blocks, however, it is quite difficult to obtain parallel lamellae when the surfaces energetically prefer the coil segments. For instance, in the case of $f = 0.4$, $\chi N = 6$, $G = 4$, $\nu = 0.5$, and $D = 6R_g$, $L^{\parallel}$ with coil segments next to the surfaces cannot be obtained until $\Delta\chi_{PW}N = \chi_{RW}N - \chi_{CW}N \geq 130$. When the surfaces attract rod segments with $\Delta\chi_{PW}N = -35$, we obtained $L^{\parallel}$ with rod segments next to the surfaces at certain D.

Figure 8 shows the density distribution of rod smectic-C phase at $f = 0.4$, $\chi N = 6$, $G = 4$, and $\nu = 0.5$ in the surface field $\Delta\chi_{PW}N = -35$ for several representative values of D, as well as the schematics of the corresponding chain configurations. It is very interesting to see that, with increasing D, the transition from rod monolayer smectic-C (mC) phase to rod bilayer smectic-C (bC) phase occurs. Here, we use symbol Θ to denote the angle between the orientation of interior rods and the lamellae normal when the interior rod lamellae exist and use Ψ to denote the angle between the orientation of rods near the film surfaces and the lamellae normal. For all four cases shown in Figure 8, the degree of rod alignment near surfaces remains unchanged ($\tilde{T}_{sur} \approx 0.77$) regardless of D and is slightly smaller than that in bulk due to confinement effect. In particular, although the walls prefer the rod blocks the rods near the surfaces are not completely parallel to them as shown in Figure 8e−h. Instead, $\Psi \approx 80°$, because rods are stretched by the coils due to junction constraint, which are repulsive with the surfaces.

In the case of $D = 2.5R_g$ shown in Figure 8a,e, the coil segments are nearly expelled from the rod domain and the rod segments form a parallel layer near each surface. As above-mentioned in the case of neutral walls, the rods prefer to form

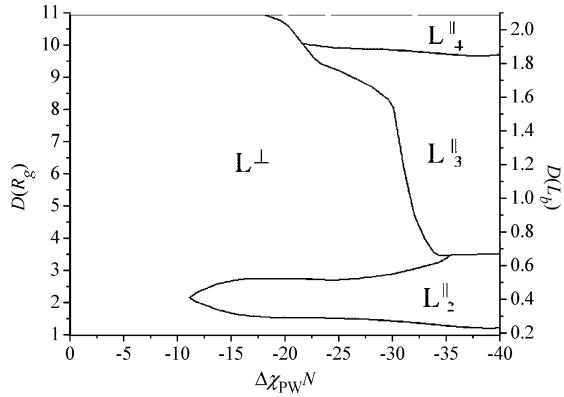

Figure 9. Phase diagram plotted in the $D-\Delta\chi_{PW}N$ plane for RC DBC with smectic-C phase formed in $f = 0.4$, $\chi N = 6$, $G = 4$, and $\nu = 0.5$ confined into two flat surfaces.

a thin layer near the surface. Moreover, the attractive interactions between rods and surfaces reinforce this effect, forming $L^{\parallel}$ in the films. With further increasing D, the coil−stretching energy F_{el} increases until rod parallel lamellae in the interior of the films occur when $D \geq 4R_g$. Subsequently, we focus on the structures of the rod parallel lamellae in the interior of the films. When $D = 4-5.5R_g$, bC $L^{\parallel}$ structure with rods almost parallel to the surfaces forms in the interior of the films. Figure 8b,f display the bC $L^{\parallel}$ phase when $D = 5R_g$. To reduce F_{el}, the rods are strongly tilted with $\Theta \approx 64°$ (much larger than that in bulk, i.e., $\Theta \approx 20°$), while leading to large rod−coil interfacial energy F_{RC}. The rod bilayer structure with small rod−coil interfacial area per chain can reduce F_{RC}, inducing a stable bC phase. It is interesting to note that the bC $L^{\parallel}$ phase is not found either in bulk or under neutral-wall confinement at the same values of χN and μN, highlighting the effect of surface preference. We also note that the bC $L^{\parallel}$ structure has a lower degree of rod alignment in the interior of the film, $\tilde{T}_{int} \approx 0.68$. It was also reported in the experiment[13] that rod−coil diblock copolymers with surface-attractive rods form bilayered smectic pattern.

When D is further increased to $6-8R_g$, both F_{el} and F_{RC} decrease, leading to the stable mC $L^{\parallel}$ phase. Parts c and g of Figure 8 show the mC $L^{\parallel}$ phase with $\Theta \approx 34°$ when $D = 7R_g = 1.33L_b$, which is larger than the bulk lamellar period $L_b = 5.25R_g$, For $D = 8.5-9.75R_g$, the bC $L^{\parallel}$ phase is obtained again. The bC $L^{\parallel}$ phase with $\Theta \approx 20°$ for $D = 9.75R_g = 1.86L_b$ is shown in Figure 8d,h. In this case, F_{el} is small due to the relatively large film thickness (less coil−stretching penalty) and the bC phase favors the rod−coil interfacial energy. Therefore, the degree of rod alignment $\tilde{T}_{int} = 0.83$, which is larger than that in bulk $\tilde{T} = 0.80$. We note that, for $D = 6 - 9.75R_g$, F_{el} remains constant, indicating that the rods align in monolayer or bilayer way with different tiling angles to ensure similar degrees of coil−stretching under different D. With further increasing D, an added rod layer emerges in the interior of the film to reduce the coil−stretching. Therefore, under the constant rod-attracted surface fields, the transitions from bC $L^{\parallel}$ to mC $L^{\parallel}$ and to bC $L^{\parallel}$ phases with increasing D is determined by the competition between F_{el} and F_{RC} both relative to the film thickness.

Moreover, we obtain a number of perpendicular lamellae $L^{\perp}$ to parallel lamellae $L^{\parallel}$ transitions shown in Figure 9 in the phase diagram in the $D-\Delta\chi_{PW}N$ plane for the rod−coil diblock copolymer thin films with bulk smectic-C phase formed in $f = 0.4$, $\chi N = 6$, $G = 4$, and $\nu = 0.5$. Although $L^{\perp}$ can freely relax to the bulk spacing with less-paid coil−stretching in thin films, the existence of surface fields prefers to form $L^{\parallel}$. The competition between the coil−stretching energy and the intense surface fields determines the phase transition between $L^{\perp}$ and $L^{\parallel}$. In contrast to the coil−coil block copolymer thin films, the self-assembled RC DBC containing the rigid rod is restricted intensely under confinement, thus $L^{\perp}$ occupy predominantly a wider range in the phase diagram. Especially when the surface fields are relatively weak such as $|\Delta\chi_{PW}N| \leq 10$, the $L^{\perp}$ phases are stable during all D we explored. Furthermore, during all our explored surface fields $L^{\perp}$ phases exist when $D \leq 1.3R_g$. With increasing $|\Delta\chi_{PW}N| \geq 11$, the parallel lamellar phases $L^{\parallel}_2$ appear when the film thickness is relatively thin as $D \approx 2.5R_g$. When surface fields are increased from $|\Delta\chi_{PW}N| = 11$ to $|\Delta\chi_{PW}N| = 40$, the area of $L^{\parallel}_2$ in the phase diagram gradually enlarges to a range of $D = 1.3-3R_g$. When the surface fields are $17 < |\Delta\chi_{PW}N| < 30$, the transitions of phase behaviors between $L^{\perp}$ and $L^{\parallel}$ are frequently observed as a function of D. We cite the case of $\Delta\chi_{PW}N = -25$ as an example: the competition between the surface field and the coil−stretching under confinement becomes more intense, leading to large transition frequency between perpendicular lamellae and parallel lamellae $L^{\perp}$ to $L^{\parallel}_2$ to $L^{\perp}$ to $L^{\parallel}_3$ to $L^{\parallel}_4$ with increasing D from $1R_g$ to $11R_g$. This agrees with the experiments by Pereira et al.[25] The abundant area of $L^{\parallel}$ in the phase diagram appears until $|\Delta\chi_{PW}N| \geq 30$, demonstrating that the strong surface fields dominate the self-assembled structures of RC DBC. Moreover, $L^{\parallel}_3$ and $L^{\parallel}_4$ are obtained in relatively large values of D. The sharp transition from $L^{\perp}$ phases to $L^{\parallel}_3$ phases occurs with increasing surface fields from $\Delta\chi_{PW}N = -30$ to $\Delta\chi_{PW}N = -35$. For a relatively strong surface field, i.e., $\Delta\chi_{PW}N = -35$ to -40, the surface field plays an important role in the self-assembled RC DBC, inducing parallel lamellae from $L^{\parallel}_2$ to $L^{\parallel}_3$ and to $L^{\parallel}_4$ with increasing D from $1.5R_g$ to $11R_g$ in our simulations. Because of the restricted rigid rod under confinement, the transitions from $L^{\parallel}_2$ to $L^{\parallel}_3$ and from $L^{\parallel}_3$ to $L^{\parallel}_4$ are almost independent of the film thickness when $\Delta\chi_{PW}N$ increases from $\Delta\chi_{PW}N = -35$ to $\Delta\chi_{PW}N = -40$. Therefore, compared with the transition of the coil−coil diblock copolymer films, the transition between $L^{\perp}$ and $L^{\parallel}$ in the $D-\Delta\chi_{PW}N$ plane is more difficult because of the intense nonbending rods constraint under confinement.

Conclusions

In this article, we present the SCFT for investigating the self-assembly of the rod−coil diblock copolymers (RC DBC) under confinement between two flat surfaces in 2D space with the so-called "masking" technique to solve the surface conditions. Maier−Saupe interaction is incorporated for describing orientational interactions between the rods and Flory−Huggins model for the enthalpic interactions between rods and coils. The orientation degree is described by a unit vector **u** discretized on the surface of a unit sphere using a set of nearly uniform triangular lattice points, i.e., icosahedron triangular mesh. In particular, this discretization is employed to numerically solve the integration of a function over sphere with relatively low computational cost, which is confirmed as an accurate and efficient way for calculating the angular quadratures of rod orientation in 3D space in contrast to normal Gaussian quadrature on the sphere. On the basis of the algorithm, the morphologies of rod−coil diblock copolymers thin films in this work are systematically investigated with the film thickness D, the surface field, different interaction degrees of the rod−coil diblock copolymers μN, χN, and the size asymmetry ratio of rods to coils β.

For neutral walls, the notable feature is that the rods are favored to form a thin layer near the surface with less-paid

entropy penalty. For smectic-C phase in bulk at $f = 0.4$, the perpendicular lamellae $L^{\perp}$ are always stable regardless of the values of film thickness, because $L^{\perp}$ can relax to their bulk spacing with less-paid coil−stretching energy F_{el} in thin films. The confinement effect can promote the microphase separation of RC DBC, inducing a higher degree of rods orientation than that in bulk. Furthermore, the parameters χN and μN have important influences on the self-assembly of rod−coil copolymers in thin films. However, when the puck-shaped phases formed in bulk in the case of $f = 0.6$ are constrained between two surfaces, the confinement effect plays an important role in the microstructures of the self-assembled RC DBC and the rods orientation. The phase behaviors of RC DBC as a function of D are far more complex, such as high transition frequency between puck-shaped phases and parallel lamellae $L^{\parallel}$. Additionally, the different puck-shaped structures under confinement are arranged in higher order than that in bulk.

For rod-attracted walls, $L^{\parallel}$ phases are obtained, and the transition of monolayer smectic-C to bilayer smectic-C phases depends on the competition between F_{el} and the rod−coil interfacial energy F_{RC} both relative to the thickness of the films. However, the transition of $L^{\perp}$ to $L^{\parallel}$ in the $D-\Delta\chi_{PW}N$ plane is more difficult than the case of coil−coil block copolymer film because of the intense constraint of nonbending rods under confinement. The competition between F_{el} and the surface fields determines the phase transition between $L^{\perp}$ and $L^{\parallel}$. $L^{\perp}$ phases occupy predominantly wider range at low surface fields, and the abundant area in the phase diagram of $L^{\parallel}$ appears until $|\Delta\chi_{PW}N| \geq 30$.

Acknowledgment. We thank financial support from the National Basic Research Program of China (Grant Nos. 2008AA032101 and 2011CB605700). Funds from the NSF of China (Grant Nos. 20990231 and 20874020) and Senior Visiting Scholar Foundation of Key Laboratory in Fudan University are also acknowledged.

References and Notes

(1) Yu, G.; Gao, J.; Hummelen, J. C.; Wudl, F.; Heeger, A. J. *Science* **1995**, *270*, 1789.
(2) Segalman, R. A.; McCulloch, B.; Kirmayer, S.; Urban, J. J. *Macromolecules* **2009**, *42*, 9205.
(3) Darling, S. B. *Energy Environ. Sci.* **2009**, *2*, 1266.
(4) Tao, Y. F.; Ma, B. W.; Segalman, R. A. *Macromolecules* **2008**, *41*, 7152.
(5) Shah, M.; Ganesan, V. *Macromolecule* **2010**, *43*, 543.
(6) Olsen, B. D.; Li, X. F.; Wang, J.; Segalman, R. A. *Macromolecules* **2007**, *40*, 3287.
(7) Olsen, B. D.; Li, X. F.; Wang, J.; Segalman, R. A. *Soft Matter* **2009**, *5*, 182.
(8) Segalman, R. A. *Mater. Sci. Eng. R-Rep.* **2005**, *48*, 191.
(9) Matsen, M. W. *J. Chem. Phys.* **1997**, *106*, 7781.
(10) Turner, M. S. *Phys. Rev. Lett.* **1992**, *69*, 1788.
(11) Segalman, R. A. *Science* **2008**, *321*, 919.
(12) Yang, G.; Tang, P.; Yang, Y. L.; Cabral, J. T. *J. Phys. Chem. B* **2009**, *113*, 14052.
(13) Park, J. W.; Cho, Y. H. *Langmuir* **2006**, *22*, 10898.
(14) Drolet, F.; Fredrickson, G. H. *Phys. Rev. Lett.* **1999**, *83*, 4317.
(15) Drolet, F.; Fredrickson, G. H. *Macromolecules* **2001**, *34*, 5317.
(16) Muller, M.; Schick, M. *Macromolecules* **1996**, *29*, 8900.
(17) Matsen, M. W.; Barrett, C. *J. Chem. Phys.* **1998**, *109*, 4108.
(18) Semenov, A. N.; Vasilenko, S. V. *Zh. Eksp. Teor. Fiz.* **1986**, *90*, 124.
(19) Saito, N.; Takahash, K; Yunoki, Y. *J. Phys. Soc. Jpn.* **1967**, *22*, 219.
(20) Hamm, M.; Goldbeck-Wood, G.; Zvelindovsky, A. V.; Sevink, G. J. A.; Fraaije, J. *Macromolecules* **2001**, *34*, 8378.
(21) Netz, P. R.; Schick, M. *Phys. Rev. Lett.* **1996**, *77*, 302.
(22) Shah, M.; Ganesan, V. *J. Chem. Phys.* **2009**, *130*, 054904.
(23) Hamm, M.; Goldbeck-Wood, G.; Zvelindovsky, A. V.; Fraaije, J. *J. Chem. Phys.* **2003**, *118*, 9401.
(24) Pryamitsyn, V.; Ganesan, V. *J. Chem. Phys.* **2004**, *120*, 5824.
(25) Pereira, G. G.; Williams, D. R. M. *Macromolecules* **2000**, *33*, 3166.
(26) Cheng, L. S.; Cao, D. P. *J. Chem. Phys.* **2008**, *128*, 74902.
(27) Nowak, C.; Vilgis, T. A. *J. Chem. Phys.* **2006**, *124*, 234909.
(28) Forsman, J.; Woodward, C. E. *Macromolecules* **2006**, *39*, 1261.
(29) Dadmun, M. D.; Muthukumar, M. *J. Chem. Phys.* **1994**, *101*, 10038.
(30) Turesson, M.; Forsman, J.; Akesson, T. *Phys. Rev. E* **2007**, *76*, 021801.
(31) Barsegov, V.; Thirumalai, A. *J. Phys. Chem. B* **2005**, *109*, 21979.
(32) Holyst, R.; Schick, M. *J. Chem. Phys.* **1992**, *96*, 730.
(33) Tang, P.; Qiu, F.; Zhang, H. D.; Yang, Y. L. *Phys. Rev. E* **2005**, *72*, 016710.
(34) Song, W. D.; Tang, P.; Zhang, H. D.; Yang, Y. L.; Shi, A. C. *Macromolecules* **2009**, *42*, 6300.
(35) Edwards, S. F. *Proc. Phys. Soc. London* **1965**, *85*, 613.
(36) Khanna, V.; Cochran, E. W.; Hexemer, A.; Stein, G. E.; Fredrickson, G. H.; Kramer, E. J.; Li, X.; Wang, J.; Hahn, S. F. *Macromolecules* **2006**, *39*, 9346.
(37) Han, W. C.; Tang, P.; Li, X.; Qiu, F.; Zhang, H. D.; Yang, Y. L. *J. Phys. Chem. B* **2008**, *112*, 13738.
(38) Singh, C.; Goulian, M.; Liu, A. J.; Fredrickson, G. H. *Macromolecules* **1994**, *27*, 2974.
(39) Tzeremes, G.; Rasmussen, K. O.; Lookman, T.; Saxena, A. *Phys. Rev. E* **2002**, *65*, 041806.
(40) Halperin, A. *Europhys. Lett.* **1989**, *10*, 549.
(41) Park, J. W.; Thomas, E. L. *Adv. Mater.* **2003**, *15*, 585.
(42) Wang, Q.; Yan, Q. L.; Nealey, P. F.; de Pablo, J. J. *J. Chem. Phys.* **2000**, *112*, 450.
(43) Meng, D.; Wang, Q. *J. Chem. Phys.* **2007**, *126*, 34902.

JP107997B